AGU PUBLICATIONS

Geophysical Research Letters

RESEARCH LETTER
10.1002/2016GL070288

Key Points:
- Interannual variations of biogeochemical features along the southwest African coast are triggered by oceanic remote equatorial forcing
- Coastal interannual fluctuations of nitrate and oxygen, controlled by physical advection processes, strongly affect primary production
- Mean vertical gradient of biogeochemical tracers shapes the oceanic biogeochemical response to Coastal Trapped Waves propagations

Supporting Information:
- Supporting Information S1
- Figure S1
- Figure S2
- Figure S3
- Figure S4
- Figure S5
- Figure S6
- Figure S7

Correspondence to:
M.-L. Bachèlery,
marie-lou.bachelery@legos.obs-mip.fr

Citation:
Bachèlery, M.-L., S. Illig, and I. Dadou (2016), Forcings of nutrient, oxygen, and primary production interannual variability in the southeast Atlantic Ocean, *Geophys. Res. Lett.*, *43*, doi:10.1002/2016GL070288.

Received 7 JUL 2016
Accepted 3 AUG 2016
Accepted article online 10 AUG 2016

Forcings of nutrient, oxygen, and primary production interannual variability in the southeast Atlantic Ocean

M.-L. Bachèlery[1], S. Illig[1,2], and I. Dadou[1]

[1]Laboratoire d'Etudes en Géophysique et Océanographie Spatiales (LEGOS), University of Toulouse, CNRS, CNES, UPS, IRD, Toulouse, France, [2]Department of Oceanography, MARE Institute, LMI ICEMASA, University of Cape Town, Cape Town, South Africa

Abstract The recurrent occurrences of interannual warm and cold events along the coast of Africa have been intensively studied because of their striking effects on climate and fisheries. Using sensitivity experimentation based on a coupled physical/biogeochemical model, we show that the oceanic remote equatorial forcing explains more than 85% of coastal interannual nitrate and oxygen fluctuations along the Angolan and Namibian coasts up to the Benguela Upwelling System (BUS). These events, associated with poleward propagations of upwelling and downwelling Coastal Trapped Waves (CTW), are maximum in subsurface and controlled by physical advection processes. Surprisingly, an abrupt change in the CTW biogeochemical signature is observed in the BUS, associated with mixed vertical gradients due to the strong local upwelling dynamics. Coastal modifications of biogeochemical features result in significant primary production variations that may affect fisheries habitats and coastal biodiversity along the southwestern African coasts and in the BUS.

1. Introduction

The Benguela Upwelling System (BUS) situated along the southwest coast of Africa from Angola to South Africa is characterized by the upwelling of nearshore deep, cold, and nutrient-rich water to the sunlit layer. This process enables the development of high primary production as well as rich and diversified marine ecosystems. It is one of the most productive areas in the world and supports the livelihoods of the population of surrounding countries [*Carr and Kearns*, 2003]. However, it is characterized by natural variability which has local implications for food security and the functioning of the marine ecosystem.

This upwelling region regularly undergoes exceptional anomalous warm and cold events at interannual period (between 14 and 18 months) that strongly impact the ecosystem development. Extreme warm events, called Benguela Niños [*Shannon et al.*, 1986], have striking effects on local marine ecosystem, fisheries [*Binet et al.*, 2001], hypoxia events [*Monteiro et al.*, 2008], and atmospheric circulation and rainfall [*Rouault et al.*, 2003]. Only a few papers have documented cold events (Benguela Niña). The latter showed that some cold events compete in magnitude with major warm episodes and their potential impact on the biota and climate needs to be investigated. The triggering mechanisms of interannual events have been highly debated for the last 10 years. Two forcing mechanisms are discussed: on one hand the role of local wind stress fluctuations in the BUS [*Richter et al.*, 2010] and on the other hand the equatorial connection through propagations of Equatorial Kelvin Waves (EKW) and then poleward Coastal Trapped Waves (CTW) [*Florenchie et al.*, 2004; *Rouault et al.*, 2007; *Lübbecke et al.*, 2010]. Recently, based on experimentation with a high-resolution oceanic regional model, *Bachèlery et al.* [2015] (hereafter BID15) have shown that ocean dynamics (sea level, temperature, and oceanic currents) along the southwest African coast at subseasonal timescales (11 days to 3 months) is mainly controlled by local forcing (in agreement with *Goubanova et al.* [2013]), while interannual events are primarily remotely forced by the equatorial dynamics. Poleward propagations of downwelling/upwelling CTW, at interannual timescales, strongly influence alongshore and vertical currents, inducing significant nearshore density and temperature variations, mostly in the subsurface.

It is yet unknown whether these strong interannual events impact biogeochemical cycles, primary production, and therefore fisheries. This is the focus of the present study which aims to quantify the impact of interannual remote equatorial forcing on the biogeochemical variability, along the southwestern

African coast, with a focus on the BUS. Using a coupled physical/biogeochemical regional model described in section 2, we will show in section 3 that remotely forced CTW control interannual nitrate and oxygen fluctuations. Then, we will describe the spatial structure of these biogeochemical tracer anomalies and depict the prevailing processes (physical and biogeochemical) accounting for their emergence. Finally, a discussion of the results, followed by implications and perspectives to this work, is given in sections 4 and 5, respectively.

2. Modeling Approach

2.1. Model Description

Our modeling approach consists of the AGRIF version [*Debreu et al.*, 2012] of the Regional Ocean Modeling System (ROMS [*Shchepetkin and McWilliams*, 2005], v3.1) coupled to the nitrogen-based Biogeochemical model developed for Eastern Boundary Upwelling System (BioEBUS) [*Gutknecht et al.*, 2013], under the southeastern Atlantic interannual configuration developed in BID15. The domain extends from 30°S to 7°N, spanning from 10°W to the western coast of Africa (Figure 1c). The horizontal resolution is 1/12° with 37 sigma vertical levels based on GEBCO_08 gridded topography. Daily surface forcing includes QuikSCAT satellite wind stress and CFSR heat and water fluxes, while 5 day dynamical Open Boundaries Conditions (OBCs) are provided by SODA reanalysis (v2.1.6). Refer to BID15 for further details and validation diagnostics, and refer to supporting information (S1) for extended information on data sets used. Monthly climatological biogeochemical OBCs are extracted from the Commonwealth Scientific and Industrial Research Organisation (CSIRO) Atlas (CARS2009) for nitrate and oxygen concentrations and from Sea-viewing Wide Field-of-view Sensor (SeaWiFS) for chlorophyll *a* (Chl *a*) concentration. Other biogeochemical fields are computed following the methodology of *Gutknecht et al.* [2013]. We used a fifth-order WENO quasi-monotone advection scheme [*Jiang and Shu*, 1996] for the biogeochemical tracers. Also, since our configuration is much larger than the one of *Gutknecht et al.* [2013], few BioEBUS biogeochemical parameters have been tuned to fit with observations, both in the BUS and in the subtropical gyre: the two stages of nitrification rate (newly 0.09 day^{-1} and 0.25 day^{-1}, respectively) as well as the decomposition rate of dissolved and particulate organic nitrogen in oxic conditions (0.004 day^{-1} and 0.001 day^{-1}, respectively) in agreement with the literature. The comparison against in situ and satellite data, provided in the supporting information (S2), indicates that our biogeochemical configuration is skillful in simulating most aspects of the mean state and interannual variability over the 2000–2008 period, with similar degree of agreement with the observations as in *Gutknecht et al.* [2013].

A total of 15 years were run for the spin-up (5 years with the physical model and 10 years with the coupled model). Then, simulations were performed over the 9 years spanning from 2000 to 2008, during which 5 day averages of physical and biogeochemical model outputs were stored.

2.2. Sensitivity Experiments

Similarly to BID15, to quantify the coastal biogeochemical response to local atmospheric forcing and to remote equatorial forcing, a set of three numerical experiments was carried out. ROMS$_{LOCAL}$ simulation is forced by real-time local surface atmospheric forcing (wind stress and heat/water fluxes) between 30°S and 4°S, while all OBCs and atmospheric forcing north of 4°S are monthly climatologies. Thus, only atmospheric effects are expected to trigger interannual variability in the coupled model. Conversely, to isolate the impact of EKW along the African west coast, we defined a paired experiment, ROMS$_{EQ}$, forced by real-time OBCs between 10°S and 7°N, while remaining OBCs and surface atmospheric forcing are monthly climatologies. Within this configuration, the southeast Atlantic interannual biogeochemical variability is only impacted by the remote equatorial connection. The last simulation (ROMS$_{REF}$) is the most realistic experiment, in which both forcings are at work.

3. Results

3.1. Coastal Interannual Variability

We first quantify the relative contribution of remote equatorial versus local forcing to the coastal biogeochemical variability.

As an illustration, Figure 1a shows the global Normalized Wavelet Power Spectra (NWPS) [*Goubanova et al.*, 2013] of coastal (0.5° width band) nutrient (nitrate) concentration for each sensitivity experiment, where mean (2000–2008) NWPS are averaged from the equator to 28°S. ROMS$_{REF}$ exhibits significant peaks of variability at subseasonal frequencies (15, 30, and 85 day^{-1}) and a marked peak at interannual timescales (450–600 day^{-1}). The latter coincides well with the sole significant peak of ROMS$_{EQ}$, while higher-frequency variability is driven

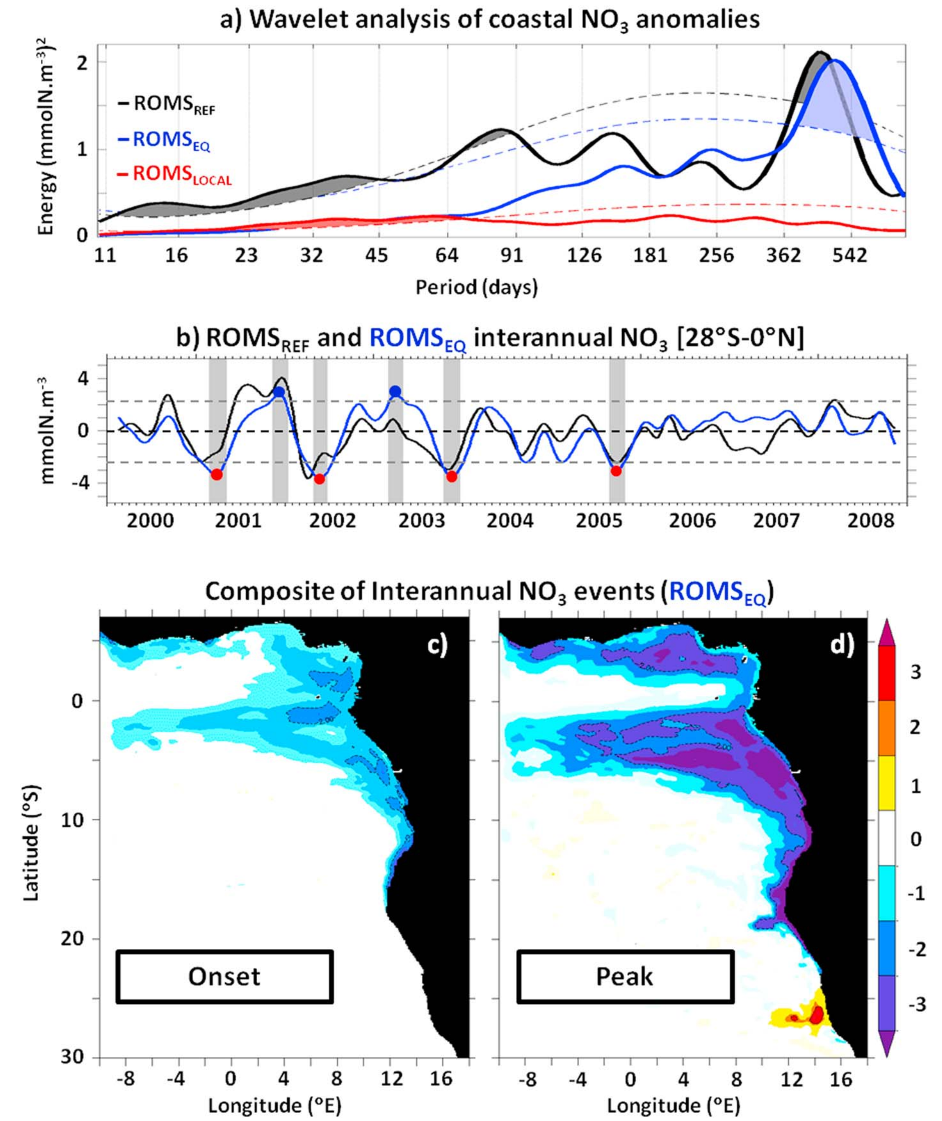

Figure 1. Nitrate concentration (mmol N m^{-3}) averaged in the first 150 m: (a) global Normalized Wavelet Power Spectrum of coastal (0.5° width band) anomalies relative the 2000–2008 seasonal cycle. NWPS computed at each latitude are averaged from 0°N to 28°S and over 2000–2008. Black, blue, and red lines correspond to ROMS$_{REF}$, ROMS$_{EQ}$, and ROMS$_{LOCAL}$ simulations, respectively. Dashed lines denote significant values at 95% confidence level. (b) Time series of ROMS$_{REF}$ (black) and ROMS$_{EQ}$ (blue) coastal (0.5° width band) interannual anomalies averaged from the equator to 28°S. Grey dashed lines denote the position of $\pm 1.25 \times$ ROMS$_{EQ}$ standard deviations. Red (blue) dots indicate peaks of major CTW warm (cold) interannual events, and grey vertical bands encircle their 2 months peak phase. (c and d) Composite maps of interannual anomalies during the onset (2.5 months before the peak) and at the peak of the events (2 month average centered around the peak), respectively. See text for composite definition.

by local atmospheric forcing (ROMS$_{LOCAL}$). The same conclusions are drawn from the analysis of coastal oxygen, Chl *a*, and depth-integrated primary production (defined here as PP) variability, however, with stronger locally forced subseasonal variability in Chl *a* and PP in the BUS. We quantified that the ROMS$_{EQ}$/ROMS$_{REF}$ ratio of GNWPS averaged along the southwest coast of Africa (0°N–28°N) at interannual frequencies is 94% for nitrate, 85% for oxygen, and 97% for PP levels. These results imply that along the southwestern African coast interannual biogeochemical variability is primarily controlled by remote equatorial forcing. Therefore, in the following, we focus on ROMS$_{EQ}$ simulation, in which CTW dominate the interannual ocean dynamics and propagate up to the model southern boundary (30°S; BID15).

The biogeochemical response to oceanic remote equatorial interannual forcing is associated with occurrences of positive and negative coastal events. Interannual downwelling CTW events (warm events in 2001

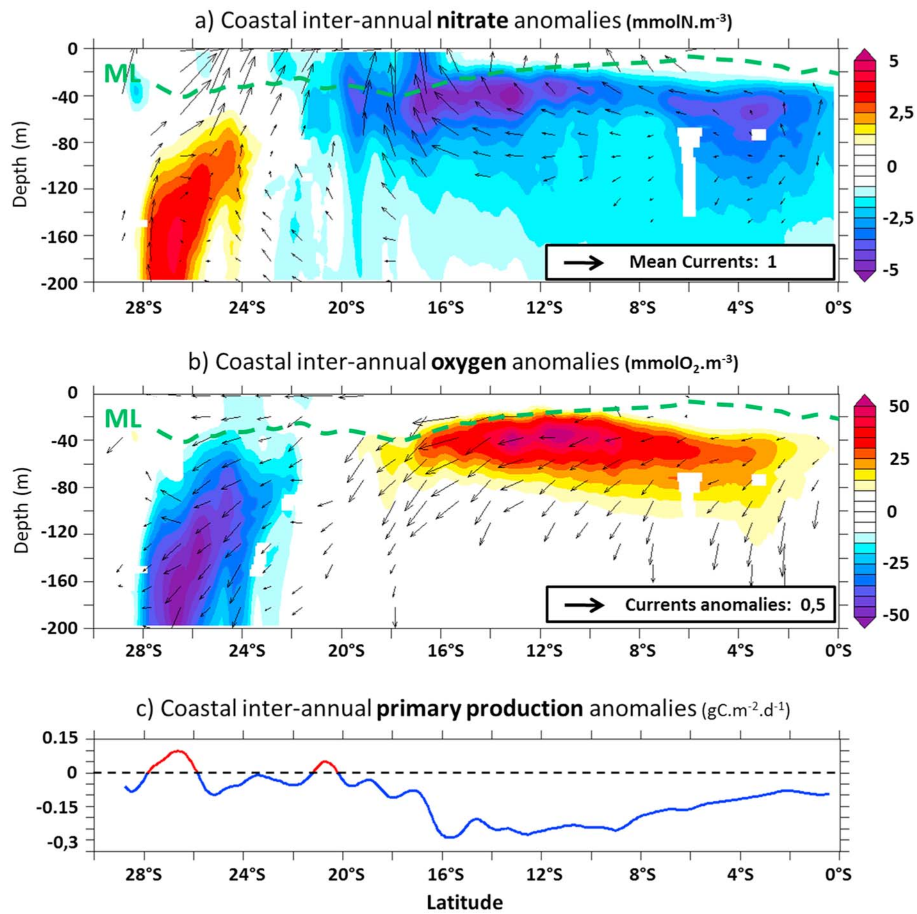

Figure 2. Composite section of interannual anomalies of coastal (0.5° width band) (a) nitrate (mmol N m^{-3}), (b) oxygen (mmol O_2 m^{-3}), and (c) depth-integrated (over the whole water column) PP (in g C m^{-2} d^{-1}) concentration of $ROMS_{EQ}$ in function of latitude and depth. In Figure 2a (Figure 2b), green dashed line denotes the mean (2000–2008) position of the mixed layer and arrows correspond to mean (interannual) vertical (m d^{-1}) and alongshore ($0.1 \times ms^{-1}$) currents. Tracers, PP, and currents were averaged over the 2 month period centered around the peak phase of selected events (cf. colored dots in Figure 1b). The maximum intensity of each event is actually traced along its poleward propagation, with a phase speed of 1 m s^{-1}.

[*Rouault et al.*, 2007], 2002, 2003/2004, and 2005, red dots in Figure 1b) trigger nutrient depletion, whereas upwelling conditions (cold events in 2001/2002 and 2003, blue dots in Figure 1b) trigger an increase in nutrients. Note that interannual anomalies are estimated as departure from the 2000–2008 monthly climatology and smoothed using a 1-2-1 monthly running weighted average (see BID15). To track the spatial and temporal evolution of interannual events, we performed composite analyses of $ROMS_{EQ}$ outputs. We used the methodology from *Illig et al.* [2014], in which positive and negative events are considered and lined up around their peak phase. We selected six events, four warm and two cold, for which averaged coastal (0.5° width band) biogeochemical tracer interannual anomalies between 0°N and 28°S exceed ±1.25 standard deviations (Figure 1b). We chose to map the downwelling phase of CTW signature. Thus, before averaging the six events, upwelling interannual anomalies are multiplied by −1 to account for their opposite effect.

Composite maps of nitrate concentration in the surface layer (0–150 m) show that during the onset of a downwelling event (Figure 1c), a weak negative anomaly starts to appear along the equator and the South African coasts up to 16°S. Two and a half months later, at the peak phase of the event (Figure 1d), the anomaly has intensified and propagated: it extends all along the southwestern African coast, reaching the BUS. Compared to the northern coastal region, an unexpected positive nitrate concentration anomaly develops in the BUS between 23°S and 28°S.

Composite of coastal latitude-depth sections at the peak phase of the events (Figure 2a) emphasizes these north-south contrasted conditions in the biogeochemical response to CTW poleward propagations showing

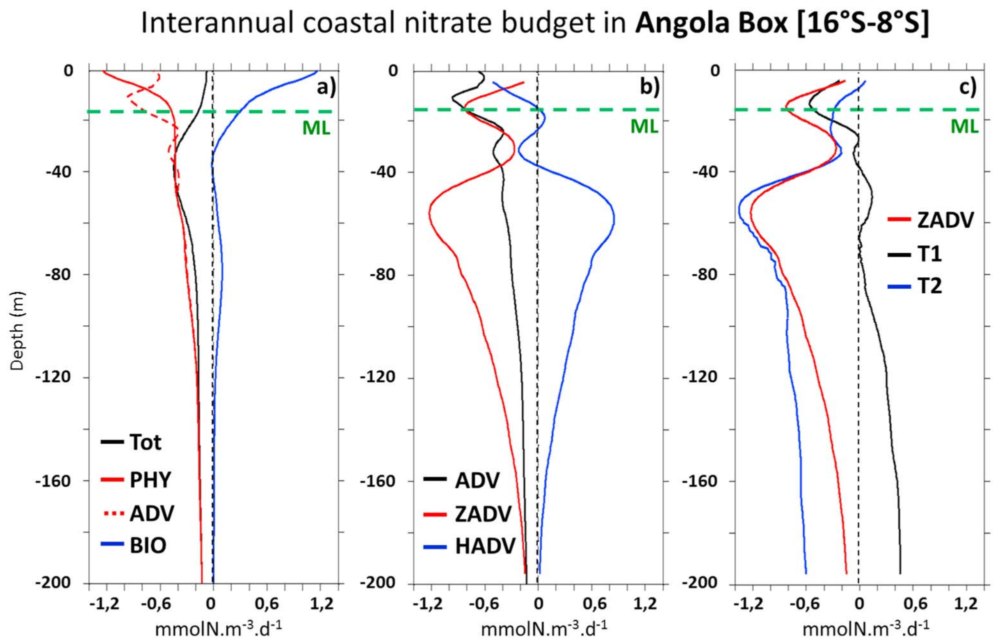

Figure 3. Composite of coastal (0.5° width band) interannual nitrate budget terms (mmol N m^{-3} d^{-1}) of $ROMS_{EQ}$: vertical profiles of tendency terms averaged over the Angola box (16°S–8°S) during the onset period of the selected events. (a) Total rate of change (TOTAL, black), summed-up contribution of physical (PHY, Red) versus biogeochemical (BIO; blue) processes, and total advection (ADV, red dashed line). (b) Total advection (ADV, black), vertical advection (ZADV, red), and horizontal advection (HADV, blue). (c) Vertical advection (ZADV, red), term 1 ($T1$, black), and term 2 ($T2$, blue) in equation (1). Horizontal green dashed line denotes the mean (2000–2008) position of the mixed layer.

opposite sign in nitrate anomalies in the BUS compared to the northern coastal area. Indeed, below the mixed layer (ML), downwelling CTW trigger negative nitrate anomalies ∼−4 mmol N m^{-3} between 0°N and 22°S, whereas they induce nitrate gain ∼+4 mmol N m^{-3} between 23°S and 28°S. The vertical distributions are also drastically different between the two regions. From 0°N to 22°S, negative nitrate anomalies are located between 120 m and the mixed layer (ML), whereas in the BUS, positive anomalies are significantly deeper (between 250 and 80 m depth).

Since nutrients and oxygen are intimately linked and closely associated with Chl *a* and PP characteristics, we obtain similar spatial distribution and temporal propagation for the dissolved oxygen (with opposite values; Figure 2b), Chl *a* concentration (not shown), as well as for PP interannual anomalies (Figure 2c). Modifications of nearshore subsurface nutrient concentration result in a significant PP variation along the Angolan and Namibian coast. We quantified that interannual remotely forced events modify the level of nitrate, oxygen, and PP along the Angolan coast up to 60%, 55%, and 30%, respectively, compared to the mean (2000–2008) levels. This impact is weaker in the Namibian enriched water with estimated ratio of 35% for nitrate, 30% for oxygen, and 10% for PP. These results highlight that interannual CTW affect coastal biogeochemical cycles as well as ecosystem richness from the equator to the northern part of the BUS. Nevertheless, the abrupt change in the biogeochemical characteristics along the poleward CTW path, resulting in a change of sign between 20°S and 22°S (Figure 2) is unexpected since in $ROMS_{EQ}$ current anomalies associated with CTW propagations (Figure 2b) show a strong reduction of the upward vertical velocities as well as an increase of the poleward alongshore currents which are continuous from 0°S to 30°S (BID15).

3.2. Processes at Work: Interannual Nitrate Budget

In order to assess the processes accounting for the interannual biogeochemical cycle variability and explain the north-south contrasting conditions associated with CTW propagations, composites of interannual online budgets of tracers of $ROMS_{EQ}$ are examined during the onset period of the event in each coastal zone: in the Angola box (16°S–8°S, Figure 3) and in the upwelling box (28°S–23°S, Figure 4). The onset period is defined as the initial period between the beginning and the peak of the event. Note that as same conclusions are drawn from O_2 budget analysis (with opposite contribution), we present only the results of the nutrient

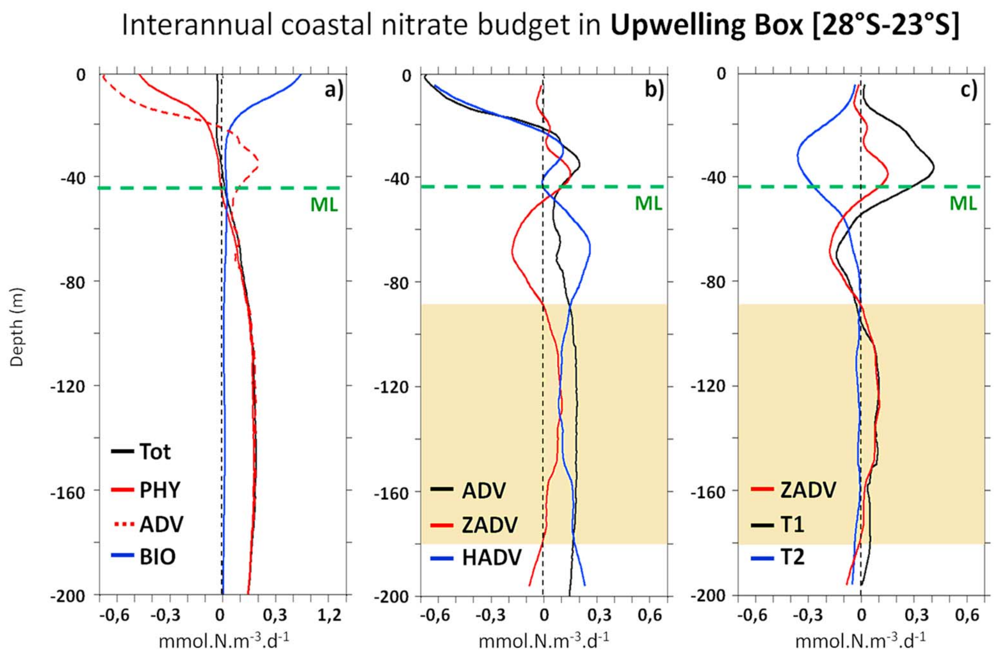

Figure 4. Same as Figure 3 but for averages over the upwelling box (28°S–23°S). Yellow shading, between 180 m and 85 m depth, highlights the area of interest.

(NO_3) budget. Processes at work can be divided into two categories: the physical processes (horizontal/vertical NO_3 advection and mixing) and biogeochemical processes (denitrification, nitrification, PP, and anammox).

In the Angola box, interannual NO_3 changes (Figure 3a, black line) are weak within the ML and result from compensation between physical and biogeochemical processes with same order of magnitude and opposite signs. In the subsurface, negative total rate of change of nitrate reflects the strong decrease in nitrate levels associated with CTW propagation (Figure 2b). Below the ML, contribution of biogeochemical processes is negligible, while physical processes, in particular the total advection term, control the vertical profile of the interannual NO_3 rate of change. Furthermore, vertical and horizontal advection terms have opposite contributions (Figure 3b): horizontal advection tends to increase nitrate levels, while vertical advection induces nitrate depletion. Indeed, during downwelling event, the increased poleward undercurrent induces stronger southward transport of enriched nutrient water. But this gain is masked by a stronger loss in nitrate caused by a reduction of the vertical advection. We then decomposed offline the interannual vertical NO_3 advection into the contribution of (1) interannual anomalies of vertical advection of anomalous nitrate concentration by seasonal vertical currents ($T1$) and (2) anomalous advection of total nitrate by vertical current anomalies ($T2$), such as

$$\mathrm{ZADV}'' = \underbrace{-\left(\overline{w} \times \frac{\partial(\mathrm{NO}_3')}{\partial z}\right)''}_{T1} \underbrace{-\left(w' \times \frac{\partial(\overline{\mathrm{NO}_3} + \mathrm{NO}_3')}{\partial z}\right)''}_{T2} \tag{1}$$

where overbars denote monthly seasonal cycle and primes denote departure from this cycle. Double prime denote interannual anomalies. Note that we carefully used the advection scheme implemented in ROMS. Results show that in the Angola box $T2$ dominates the nitrate interannual advection (Figure 3c), while $T1$ contributes to a weak gain. Consequently, along the Angolan coast during interannual events, the nitrate loss in subsurface is controlled by the reduction in the upward transport of deep nutrient-rich water.

Farther poleward, interannual subsurface nitrate anomalies associated with CTW turn from negative to positive. This nitrate gain is depicted by a positive total rate of change in the BUS (Figure 4a). Similarly to the northern part, the physical and biogeochemical processes compensate each other in the ML, resulting in weak NO_3 changes. Below the ML, physical processes—specifically the advection terms—are the main contributors to interannual nitrate anomalies, while biogeochemical processes remain negligible. In the BUS, between 180 m and 85 m depth, it is actually the sum of the horizontal and vertical fluxes which contributes to the total NO_3 flux (Figure 4b, yellow shaded area). Both processes contribute to nitrate gain. Similar to the Angola box, positive nitrate horizontal advection is associated with the increased poleward alongshore currents in the subsurface (Figure 3b). Unexpectedly, compared to the northern counterpart, the interannual vertical advection contributes here to nitrate inputs, while interannual vertical velocities are still negative (Figure 2b), characteristics of the upwelling reduction along the downwelling CTW propagation. The vertical advection decomposition from equation (1) (Figure 4c) highlights that $T1$ contributes to nitrate gain in the BUS, similarly to the Angola box. Distinguishingly, under similar vertical current anomalies (Figure 2b), $T2$ has relatively smaller amplitude in the BUS, compared to the northern area. This is due to the strong and permanent local upwelling dynamics that drastically reduces the coastal nitrate vertical gradient in the BUS. Thus, the decrease in vertical velocity does not have a strong vertical gradient in nitrate to work on, such as the signature of the anomalous reduction in nitrate vertical transport ($T2$) becomes small compared to the positive gain associated with seasonal transport of the anomalous vertical nitrate gradient ($T1$). This emphasizes the importance of the mean vertical gradient of tracers in the biogeochemical response to interannual CTW propagations. To summarize, the positive subsurface nutrient gain in the BUS is explained by the horizontal advection of nitrate-rich water from the equator toward the pole, concomitant with vertical advection of deep nutrient-rich water.

4. Discussion

At interannual timescales, we showed that the equatorial connection has a strong impact on nutrient variability along the southwestern African coasts compared to local atmospheric forcing (Figure 1a). Thus, $ROMS_{REF}$ is expected to depict a very similar spatiotemporal interannual variability compared to $ROMS_{EQ}$. This is indeed the case: $ROMS_{REF}$ and $ROMS_{EQ}$ share similar features in nutrients (Figure 1b), oxygen, and PP (not shown) distribution and propagation characteristics. In particular, $ROMS_{REF}$ latitude-depth composite sections at the peak phase of strong interannual events in nitrate, oxygen, and PP (not shown) portray the north-south contrasting conditions between Angolan and BUS coastal regions (similarly to Figure 2). This is particularly true for the 2001 and 2001/2002 interannual events, in agreement with Chl *a* observations (see Figure S6 in the supporting information). However, for some particular events (2003 and 2004) notable differences in the amplitude of the tracers and PP coastal anomalies are reported. Thus, although the remote equatorial forcing dominates the coastal biogeochemical variability, other processes modulate the remotely forced interannual variability in the most realistic simulation.

While local atmospheric forcing remains weak at interannual timescales, intermittent wind variations along the equator and along the coast can induce significant variability, which can be in phase or out of phase with the remote equatorial forcing. Indeed, based on similar sensitivity experiments, BID15 showed that weak interannual anomalies triggered by local atmospheric forcing can, however, modulate the intensity of remotely forced temperature events and affect the maximum poleward latitude at which interannual CTW can be detected. Also, interannual wind variations in the Gulf of Guinea can force EKW and in turn trigger CTW propagation, which modulates the coastal interannual event intensity (BID15). Prescribing real-time atmospheric forcing in the equatorial band (north of 4°S) in $ROMS_{EQ}$ reveals that the effects of remote equatorial forcing add linearly to fluctuations associated with local atmospheric forcing in $ROMS_{LOCAL}$ to reconstitute most of the reference coastal biogeochemical signal in $ROMS_{REF}$ between the equator and 26°S (not shown). However, unlike density variations (BID15), in this latitudinal range, some differences between $ROMS_{REF}$ and $ROMS_{EQ}$ cannot be attributed to local atmospheric forcing. This is the case during the year 2004 where the interannual remotely forced event is stopped unexpectedly at 20°S. This suggests that interactions between short-term scales (at which the local forcing is dominant; Figure 1a [*Goubanova et al.*, 2013]) and longer-term variability (at which the equatorial forcing prevails) may occasionally play a role in biogeochemical tracer signature. Noteworthy, poleward of 26°S, $ROMS_{REF}$ and $ROMS_{EQ}$ signals are less consistent. While $ROMS_{REF}$ is affected by interannual variability at 30°S, this is not the case for $ROMS_{EQ}$, where monthly climatology has been prescribed at its southern boundary (cf. section2.2). Thus, part of the biogeochemical interannual variability in $ROMS_{REF}$ from 30°S to 26°S is controlled by modulations of the equatorward Benguela current variability (fed by the Agulhas Current and the South Atlantic Current) and its associated mesoscale activity (BID15).

Identifying the dominant forcings of coastal interannual events is a critical issue for their prediction and will be particularly relevant to support ecosystem and fisheries management in the BUS. All forcings (EKW, local winds, and southern entrances at 30°S) are independent, with their own timescales of variability. While remote equatorial forcing activity is a skillful proxy to forecast coastal temperature extreme events by about 1 month in advance (R. A. Imbol Koungue et al., Role of Interannual Kelvin wave propagations in the equatorial Atlantic on the Angola Benguela current system, submitted to *Journal of Geophysical Research: Oceans*, 2016), this is not the case for the ocean variability at the southern tip of Africa, as well as for the local atmospheric forcing which impacts preferentially shorter-term variability. Fortunately, this study highlights that interannual biogeochemical coastal events are primarily controlled by the equatorial connection (Figure 1a). This should allow forecasting their occurrences and anticipate the associated patterns in nutrients, oxygen, and PP, but not their magnitude which can be modulated by local atmospheric variability.

5. Conclusions

The BUS has long been recognized as a high productive area and fisheries reservoir on which several developing countries depend. Yet sensitivity experiments with a coupled model show that poleward propagations of remotely forced CTW induce drastic coastal nutrients and oxygen fluctuations — ∼60% to ∼30% of the mean levels — from the equator toward the BUS. These fluctuations are triggered by physical processes and in particular the advection terms. These fluctuations may strongly affect fisheries habitats and coastal biodiversity, since nutrient availability in the euphotic layer has important repercussion on Chl *a* and PP. We quantified that these interannual events, which can last up to 6 months, contribute up to 30% of the mean PP levels along the Angolan coast and 10% in the BUS enriched water. Furthermore, the associated variation in the subsurface oxygen content along the shelf may also affect the extension of the oxygen minimum zone and enhance natural hypoxia, which would increase the effects of remote equatorial forcing on the ecosystem. Indeed, the impacts of hypoxic events can vary from major species displacements to mortalities associated with nonviable conditions. It can also result in catastrophic loss in fisheries by poisoning due to episodic sulphide eruptions (H_2S). Since H_2S production depends on the biogeochemical settings (i.e., oxygen and nitrate levels), the connection between the remote equatorial forcing and the anomalous episodic emissions of toxic gases in the BUS, as well as their potential impact on ecosystems and their forecast, will be the topic of our next research efforts.

Acknowledgments
This work was supported by a grant (OSTST-TOSCA project EBUS-SOUTH) from the Centre National d' Etudes Spatiales, France (CNES) and by a PhD fellowship from the Centre National de la Recherche Scientifique (CNRS). We thank ICEMASA (IRD) and ATUPS (Université Paul Sabatier) for financial support allowing a 6 month visit in the Department of Oceanography of UCT in Cape Town, South Africa. The authors wish to thank the latter for its warm welcome, helpful discussions, and new friendships. We acknowledge B. Le Vu and V. Garçon for sharing their preliminary results, as well as P. Penven and B. Dewitte for fruitful discussions. All data used in this study (for model forcing and validation) are publicly available, and detailed information are provided in the supporting information (S1). CERSAT, CSIRO, Texas A&M University, and NASA are thanked for development and distribution of these data sets. ROMS/BioEBUS model was downloaded from the ROMS_AGRIF public repository at http://www.romsagrif.org. Model grid, forcings, and initial conditions were built using the ROMS_TOOLS package [*Penven et al.*, 2007]. This work was performed using HPC resources from CALMIP (grant 2015-2016 - P1134). We would like to thank the two anonymous reviewers for their thorough reading and their constructive comments, which helped improve the quality of this paper.

Acronyms

BID15	*Bachèlery et al.* [2015].
BUS	Benguela Upwelling System.
EKW	Equatorial Kelvin Waves.
CTW	Coastal Trapped Waves.
GEBCO	General Bathymetric Chart of the Oceans.
QuikSCAT	Quik SCAtterometer Satellite.
CFSR	NCEP Climate Forecast System Reanalysis.
SODA	Simple Ocean Data Assimilation.
CSIRO	Commonwealth Scientific and Industrial Research Organisation.
WENO	Weighted Essentially Non-Oscillatory.
PP	depth-integrated Primary Production.

References

Bachèlery, M.-L., S. Illig, and I. Dadou (2015), Interannual variability in the South-East Atlantic Ocean, focusing on the Benguela Upwelling System: Remote versus local forcing, *J. Geophys. Res. Oceans*, *121*, 284–310, doi:10.1002/2015JC011168.

Barlow, R., T. Lamont, B. Mitchell-Innes, M. Lucas, and S. Thomalla (2009), Primary production in the Benguela ecosystem, 1999–2002, *Afr. J. Mar. Sci.*, *31*, 97–101.

Binet, D., B. Gobert, and L. Maloueki (2001), El Niño-like warm events in the Eastern Atlantic (6°N, 20°S) and fish availability from Congo to Angola (1964–1999), *Aquat. Living Resour.*, *14*(2), 99–113.

Carr, M.-E., and E. J. Kearns (2003), Production regimes in four Eastern Boundary Current systems, *Deep Sea Res., Part II*, *50*(22–26), 3199–3221.

Carton, J. A., and B. S. Giese (2008), A reanalysis of ocean climate using Simple Ocean Data Assimilation (SODA), *Mon. Weather Rev.*, *136*(8), 2999–3017.

Carton, J. A., G. Chepurin, X. Cao, and B. Giese (2000), A simple ocean data assimilation analysis of the global upper ocean 1950–95. Part I: Methodology, *J. Phys. Oceanogr.*, *30*(2), 294–309.

Carton, J. A., B. S. Giese, and S. A. Grodsky (2005), Sea level rise and the warming of the oceans in the Simple Ocean Data Assimilation (SODA) ocean reanalysis, *J. Geophys. Res.*, *110*, C09006, doi:10.1029/2004JC002817.

Debreu, L., P. Marchesiello, P. Penven, and G. Cambon (2012), Two-way nesting in split-explicit ocean models: Algorithms, implementation and validation, *Ocean Model.*, *49-50*, 1–21.

Dunn, J. R., and K. R. Ridgway (2002), Mapping ocean properties in regions of complex topography, *Deep Sea Res., Part I*, *49*(3), 591–604.

Florenchie, P., C. J. C. Reason, J. R. E. Lutjeharms, M. Rouault, C. Roy, and S. Masson (2004), Evolution of interannual warm and cold events in the Southeast Atlantic Ocean, *J. Clim.*, *17*(12), 2318–2334.

Fréon, P., M. Barange, and J. Arístegui (2009), Eastern boundary upwelling ecosystems: Integrative and comparative approaches, *Prog. Oceanogr.*, *83*(1–4), 1–14.

Goubanova, K., S. Illig, E. Machu, V. Garçon, and B. Dewitte (2013), SST subseasonal variability in the central Benguela upwelling system as inferred from satellite observations (1999–2009), *J. Geophys. Res. Oceans*, *118*, 4092–4110, doi:10.1002/jgrc.20287.

Gutknecht, E., et al. (2013), Coupled physical/biogeochemical modeling including O_2-dependent processes in the Eastern Boundary Upwelling Systems: Application in the Benguela, *Biogeosciences*, *10*(6), 3559–3591.

Illig, S., B. Dewitte, K. Goubanova, G. Cambon, J. Boucharel, F. Monetti, C. Romero, S. Purca, and R. Flores (2014), Forcing mechanisms of intraseasonal SST variability off central Peru in 2000–2008, *J. Geophys. Res. Oceans*, *118*, 3548–3573, doi:10.1002/2013JC009779.

Jiang, G. S., and C. W. Shu (1996), Efficient implementation of weighted ENO schemes, *J. Comput. Phys.*, *126*(1), 202–228.

Kuypers, M. M. M., G. Lavik, D. Woebken, M. Schmid, B. M. Fuchs, R. Amann, B. B. Jøorgensen, and M. S. M. Jetten (2005), Massive nitrogen loss from the Benguela upwelling system through anaerobic ammonium oxidation, *Proc. Natl. Acad. Sci. U.S.A.*, *102*(18), 6478–6483.

Lavik, G., et al. (2009), Detoxification of sulphidic African shelf waters by blooming chemolithotrophs, *Nature*, *457*(7229), 581–584.

Liu, W. T., W. Q. Tang, and P. S. Polito (1998), NASA scatterometer provides global ocean-surface wind fields with more structures than numerical weather prediction, *Geophys. Res. Lett.*, *25*(6), 761–764.

Lübbecke, J. F., C. W. Böning, N. S. Keenlyside, and S.-P. Xie (2010), On the connection between Benguela and equatorial Atlantic Niños and the role of the South Atlantic Anticyclone, *J. Geophys. Res.*, *115*, C09015, doi:10.1029/2009jc005964.

McClain, C. R., M. L. Cleave, G. C. Feldman, W. W. Gregg, S. B. Hooker, and N. Kuring (1998), Science quality SeaWiFS data for global biosphere research, NASA/Goddard Space Flight Center, *Sea Technol.*, *39*, 10–16.

Monteiro, P. M. S., A. K. van der Plas, J.-L. Mélice, and P. Florenchie (2008), Interannual hypoxia variability in a coastal upwelling system: Ocean-shelf exchange, climate and ecosystem-state implications, *Deep Sea Res., Part I*, *55*(4), 435–450.

Ohde, T., H. Siegel, and M. Gerth (2007), Validation of MERIS Level 2 products in the Baltic Sea, the Namibian coastal area and the Atlantic Ocean, *Int. J. Remote Sens.*, *28*(3–4), 609–624.

O'Reilly, J. E., et al. (2000), *Ocean Color Chlorophyll a Algorithms for SeaWiFS, OC2, and OC4: Version 4. SeaWiFS Postlaunch Calibration and Validation Analyses, Part 3. NASA Tech. Memo. 2000-206892*, C. R. McClain (Ed.), vol. 11, pp. 9–23, NASA Goddard Space Flight Center, Greenbelt, Md.

Penven, P., P. Marchesiello, L. Debreu, and J. Lefevre (2007), Software tools for pre- and post-processing of oceanic regional simulations, *Environ. Model Softw.*, *23*, 660–662.

Richter, I., S. K. Behera, Y. Masumoto, B. Taguchi, N. Komori, and T. Yamagata (2010), On the triggering of Benguela Niños: Remote equatorial versus local influences, *Geophys. Res. Lett.*, *37*, L20604, doi:10.1029/2010GL044461.

Ridgway, K. R., J. R. Dunn, and J. L. Wilkin (2002), Ocean interpolation by four-dimensional weighted least squares: Application to the waters around Australasia, *J. Atmos. Oceanic Technol.*, *19*(9), 1357–1375.

Rouault, M., P. Florenchie, N. Fauchereau, and C. J. C. Reason (2003), South East tropical Atlantic warm events and southern African rainfall, *Geophys. Res. Lett.*, *30*(5), 8009, doi:10.1029/2002GL014840.

Rouault, M., S. Illig, C. Bartholomae, C. J. C. Reason, and A. Bentamy (2007), Propagation and origin of warm anomalies in the Angola Benguela upwelling system in 2001, *J. Mar. Syst.*, *68*(3-4), 473–488.

Saha, S., et al. (2010), The NCEP climate forecast system reanalysis, *Bull. Am. Meteorol. Soc.*, *91*(8), 1015–1057.

Shannon, L. V., A. J. Boyd, G. B. Brundrit, and J. Taunton-Clark (1986), On the existence of an El Niño-type phenomenon in the Benguela System, *J. Mar. Res.*, *44*(3), 495–520.

Shchepetkin, A. F., and J. C. McWilliams (2005), The regional oceanic modeling system (ROMS): A split-explicit, free-surface, topography-following-coordinate oceanic model, *Ocean Model.*, *9*(4), 347–404.

Zabel, M. (2003), *Report and Preliminary Results of METEOR Cruise M 57/2, Walvis Bay-Walvis Bay, 11.02-12.03.2003*, Dep. Geosci., Bremen Univ., Bremen, Germany.

Supporting Information for

"Forcings of nutrient, oxygen and primary production interannual variability in the South-East Atlantic Ocean"

M.-L. Bachèlery[1], S. Illig[1,2], and I. Dadou[1]

[1]Laboratoire d′Etudes en Géophysique et Océanographie Spatiales (LEGOS), University of Toulouse, CNRS, CNES, UPS, IRD, Toulouse, Midi-Pyrénée, France.

[2]Department of Oceanography, MARE Institute, LMI ICEMASA, University of Cape Town, Cape Town, Rondebosh, South Africa.

Contents

Introduction

This supporting information provides additional information about datasets used in this study as well as figures that show the coupled physical / biogeochemical model performances for the realistic simulation $ROMS_{REF}$. Descriptions of the individual figures follow bellow.

S1: Datasets information

For forcing and evaluation of model performances, numerous *in situ* and satellite data are used, along with reanalysis outputs.

Satellite datasets

QuikSCAT: We use gridded Sea Winds scatterometer wind stress observations from NASA satellite QuikSCAT [*Liu et al.*, 1998]. Daily global maps are available over the 2000-2008 period with a resolution of 0.5°×0.5°, provided by the French Centre ERS d'Archivage et de Traitement (CERSAT, *http://cersat.ifremer.fr*). To force our ROMS simulations, zonal and meridional wind stress components have been linearly interpolated on our 1/12°model grid. Note that, in order to fill in the QuikSCAT blind coastal zone, an extrapolation of the QuikSCAT momentum fluxes was performed using a simple near-neighbor procedure.

Corresponding author: Marie-Lou Bachèlery, `marie-lou.bachelery@legos.obs-mip.fr`

SeaWiFS: Surface chlorophyll-a concentrations are provided by the Sea-viewing Wide Field-of-view Sensor (SeaWiFS) products of level 3-binned data (9 km, version 4) [*O'Reilly et al.*, 2000], over the 2000-2008 period. Data are processed by NASA Goddard Space Flight Center and distributed by Distributed Active Archive Center (DAAC, [*McClain et al.*, 1998]; *http://oceancolor.gsfc.nasa.gov/SeaWiFS*). Monthly data are linearly regridded from the original 0.0879°×0.0879° grid onto the 1/12° model grid, for comparison with surface simulated Chlorophyll-a.

Reanalysis

SODA oceanic Reanalysis: The outputs of the Simple Ocean Data Assimilation reanalysis (SODA, version 2.1.6) are used as physical initial and open boundary conditions of our regional model configuration [*Bachèlery et al.*, 2015]. SODA combines the Los Alamos implementation of the POP (Parallel Ocean Program) model with data assimilation of all available data from hydrographic stations, expendable bathythermographs and floats [*Carton et al.*, 2000; *Carton and Giese*, 2008; *Carton et al.*, 2005]. Homogeneous temporal series of 5 day averages of temperature, salinity, sea level and oceanic currents, with a horizontal resolution of 0.5°×0.5° and 40 verticals levels are available at *http://www.atmos.umd.edu/ ocean/data.html*.

CFSR atmospheric Reanalysis: For our model forcing [*Bachèlery et al.*, 2015], daily averages of specific humidity, 2 m air temperature, 10 m wind speed, shortwave, longwave heat fluxes, precipitations and Sea Surface Salinity are provided by the National Center of Environmental Prediction-Climate Forecast System Reanalysis (NCEP-CFSR) [*Saha et al.*, 2010]. CFSR is a coupled (ocean/atmosphere/land surface/sea ice) data assimilation system using observed SST, temperature, and salinity profiles from MBT, XBT, CTD, Argo, and TAO. NCEP-CFSR outputs are available on a 0.5°×0.5° horizontal grid at different temporal resolutions (from hourly to monthly) over the 31 year period extending from 1979 to 2009.

In situ datasets

CSIRO Atlas of Regional Seas 2009: Monthly nitrate and oxygen climatologies of the 2009 Commonwealth Scientific and Industrial Research Organisation (CSIRO) Atlas of Regional Seas (CARS2009) are available at *www.cmar.csiro.au/cars*. CARS 2009 gridded maps covers the global ocean on a 0.5°×0.5° horizontal grid with 79 vertical levels. It combines all available oceanic data over the last 50 years using rigorous quality controls and an adaptive-length-scale loess mapper to maximize resolution in data-rich regions (see *Ridgway et al.* [2002]; *Dunn and Ridgway* [2002] for more details CARS2009 input data sources and method.

***In situ* data from cruises**: Several *in situ* measurements of nitrate and oxygen were used to evaluate the performances of the $ROMS_{REF}$ simulation along the coast of southwest Africa. Data were collected during the M57/2 of R/V Alexander expedition in February 2003 [*Zabel*, 2003; *Kuypers et al.*, 2005] and the AHAB1 of R/V Alexander von Humboldt in January 2004 [*Lavik et al.*, 2009] over the Namibian Upwelling System along sections at different latitudes ranging from 23°S to 27°S.

GEBCO_08 topography: Model topography was derived from the GEneral Bathymetric Chart of the Ocean (GEBCO) at 30 arc-seconds grid (GEBCO_08) global elevation database (*http://www.gebco.net*).

S2: Model Validation

The most realistic simulation performances are evaluated against *in situ* and satellite data. Extended description of the datasets used can be found in the previous section (see S1- Datasets information).

Biogeochemical mean state (averaged over the 2000-2008 period)

The model reasonably reproduces the spatial pattern of minimum O_2 concentrations, compared to the CSIRO 2009 Atlas (CARS), portraying the intrusion of low dissolved oxygen equatorial waters along the southwestern African coast from 15°S to 26°S (**FigS1**). However, the model overestimates O_2 concentrations over the shelf between 24°S and 30°S, most likely due to the lack of coupled water-sediment processes which are not taken into account in the current version of the biogeochemical model BioEBUS. Overall, over the model domain (7°N-30°S and 10°W-18°E) the mean modeled O_2 levels show statistically fair agreements with CARS climatology with spatial correlation coefficient averaged over the top 200-meters (the whole water column) of 0.91 (0.92) and mean biases of -0.38 (-0.81) $mmolO_2.m^{-3}$ (**FigS4** - Taylor diagram).

The spatial pattern of the modeled nutrient (nitrate) concentrations is in good agreement with CARS climatology (**FigS2**). Maximum errors ($\sim$6 $mmolN.m^{-3}$) are located along the southwestern African coast between 24°S and 30°S and result also from the lack of coupled water-sediment interactions. Despite this bias, over the whole domain the model simulates a realistic mean nitrate concentration compared to CARS, with a spatial correlation coefficient averaged over top 200-meter (whole water column) between model and observations of 0.96 (0.98) and a mean bias of -0.98 (-0.83) $mmolN.m^{-3}$(**FigS4** - Taylor diagram).

The modeled surface chlorophyll-a (Chla) concentrations share most characteristics of SeaWiFS satellite climatology [*McClain et al.*, 1998] (**FigS3.ab**): high coastal values typical for coastal upwelling area from 16°S to 30°S along the southwestern African coast, as well as relatively low values off-shore, in the subtropical South-Atlantic gyre. Otherwise, the model slightly underestimates coastal surface Chla concentrations by 1.5 mgChl.m^{-3}, along the southwestern African coast. Despite this bias, $ROMS_{REF}$ is in good agreement with SeaWiFS climatology showing a spatial correlation coefficient of 0.93 and a mean bias of 0.076 mgChl.m^{-3} (**FigS4** - Taylor diagram).
Note that oxygen, nitrate and Chla statistics illustrated in the Taylor Diagram (**FigS4**) are similar to results obtained in *Gutknecht et al.* [2013].

Biogeochemical Interannual variability

To gain more confidence in the model performances at interannual timescales, we compared modeled vertical profiles selected for two different periods (February 2003 and January 2004) at four different locations (23°S, 25°S, 26°S and 27°S) to corresponding *in situ* data (from M57/2 and AHAB1 cruises) [*Zabel*, 2003; *Kuypers et al.*, 2005; *Lavik et al.*, 2009] and CARS vertical profiles. **Figure S5** shows typical profiles of oxygen and nitrate concentrations in the coastal upwelling with a pronounced reduction of oxygen concentrations between 200 *in situ* and 300-meter depth. The model reasonably reproduces the general spatial pattern of oxygen and nitrate concentrations and agree well with data within a range of errors $\sim\pm 20$ mmolO_2.m^{-3} and ± 5 mmolN.m^{-3}, respectively. These results are also in better agreement with CARS climatology than those presented in *Gutknecht et al.* [2013].
The interannual variability of model and satellite (SeaWiFS) surface Chla on the shelf (averaged over the 100km-width band from the coast, between 10°S to 25°S) over the 2000-2008 period is shown in **Figure S3.c**. The simulated interannual Chla is not always in good agreement with the satellite observations with an estimated correlation coefficient between $ROMS^{REF}$ and SeaWiFS timeseries of 0.37 (not statistically significant). This discrepancy may be due to several aspects. First, note that Chla estimates from remote sensing ocean color data are not so accurate compared to *in situ* measurements. In particular, it was shown that in the south-eastern Atlantic they have relative mean errors of 30% (∼18% for the specific year 2003, *Ohde et al.* [2007]) compared with *in situ* data and are very sensitive to clouds, especially in the Northern Benguela during winter season [*Ohde et al.*, 2007]. Also, the ocean color sensor of SeaWiFS has considerably less data in 2008 due to technical problems. Thus, we also draw the reader attention to the fact that it is advisable to place a caveat on the observed interannual

Chla estimations, as satellites products contain numerous missing values due to the cloud cover. This renders difficult the estimation of observed coastal interannual variability, which can be detrimental for our model validation exercise. Despite this bias, both time series show interannual fluctuations within -0.8 and 1.6 mgChl.m^{-3} with comparable Root Mean Square (RMS) (ROMS^{REF}: 0.12 mgChl.m^{-3} and SeaWiFS: 0.16 mgChl.m^{-3}). More importantly, major interannual events such as the 2001 Benguela Niño (BID15, [*Rouault et al.*, 2007]) and the cold event in 2001/2002 are relatively well captured by the model as compared to SeaWiFS interannual time series. This is illustrated in **Figure S6** which shows the interannual variations of coastal Chla from the equator to 30°S, in April 2001 and December/January 2001/2002 for ROMS$_{REF}$ and SeaWiFS satellite data. Despite some biases and noise in SeaWiFS coastal interannual estimated, the model shows similar patterns as the observations. In particular, both model and SeaWiFS exhibit the north-south contrasting conditions described in section 3.1 and 3.2, characterized by a Chla depletion (increase) from 25°S to 0°S and a small choloropyll-a increase (depletion) south of 25°S in **Figure S6.a** (**Fig S6.b**).
Modeled Primary Production (PP) was compared with *in situ* data obtained during a summer cruise on February-March 2002 [*Barlow et al.*, 2009] (**FigS7**). Even if the model underestimates some extreme values of PP, the spatial variability as well as the PP magnitude are well captured by the model.

In conclusion, results show that the model is skillful in simulating the southeastern Atlantic Ocean mean state and interannual variability in the ROMS$_{REF}$ simulation.

References

Bachèlery, M.-L., S. Illig, and I. Dadou (2015), Interannual variability in the South-East Atlantic Ocean, focusing on the Benguela Upwelling System: Remote versus local forcing, *J. Geophys. Res. Oceans*, *121*(1), 284-310.

Barlow, R., T. Lamont, B. Mitchell-Innes, M. Lucas, and S. Thomalla (2009), Primary production in the Benguela ecosystem, 1999-2002, *Afr. J. Mar. Sci.*, *31*, 97-101.

Carton, J. A., and B. S. Giese (2008), A reanalysis of ocean climate using simple ocean data assimilation (SODA), *Mon. Weather Rev.*, *136*(8), 2999-3017.

Carton, J. A., G. Chepurin, X. Cao, and B. Giese (2000), A simple ocean data assimilation analysis of the global upper ocean 1950-95. Part I: Methodology, *J. Phys. Oceanogr.*, *30*(2), 294-309.

Carton, J. A., B. S. Giese, and S. A. Grodsky (2005), Sea level rise and the warming of the oceans in the Simple Ocean Data Assimilation (SODA) ocean reanalysis, *J. Geophys. Res.*, *110*, C09006.

Dunn, J. R., and K. R. Ridgway (2002), Mapping ocean properties in regions of complex topography, *Deep Sea Res. Part I*, *49*(3), 591-604.

Gutknecht, E., I. Dadou, B. Le Vu, G. Cambon, J. Sudre, V. Garçon, E. Machu, T. Rixen, A. Kock, A. Flohr, A. Paulmier, and G. Lavik (2013), Coupled physical/biogeochemical modeling including O2-dependent processes in the Eastern Boundary Upwelling Systems: application in the Benguela, *Biogeosciences*, *10*(6), 3559-3591.

Kuypers, M. M. M., G. Lavik, D. Woebken, M. Schmid, B. M. Fuchs, R. Amann, B. B. Jøorgensen, and M. S. M. Jetten (2005), Massive nitrogen loss from the Benguela upwelling system through anaerobic ammonium oxidation, *Proc. Natl. Acad. Sci. U.S.A.*, *102*(18), 6478-6483.

Lavik, G., T. Stührmann, V. Brüchert, A. Van der Plas, V. Mohrholz, P. Lam, M. M. Zligmann, B. M. Fuchs, R. Amann, U. Lass, and M. M. M. Kuypers (2009), Detoxification of sulphidic African shelf waters by blooming chemolithotrophs, *Nature*, *457*(7229), 581-584.

Liu, W. T., W. Q. Tang, and P. S. Polito (1998), NASA scatterometer provides global ocean-surface wind fields with more structures than numerical weather prediction, *Geophys. Res. Lett.*, *25*(6), 761-764.

McClain, C. R., M. L. Cleave, G. C. Feldman, W. W. Gregg, S. B. Hooker, and N. Kuring (1998), Science Quality SeaWiFS Data for Global Biosphere Research, NASA/Goddard Space Flight Center, *Sea Technol.*, *39*, 10-16.

Ohde, T., H. Siegel and M. Gerth (2007) Validation of MERIS Level 2 products in the Baltic Sea, the Namibian coastal area and the Atlantic Ocean, International Journal of Remote Sensing, 28:3-4, 609-624.

O'Reilly, J. E. et al (2000), Ocean color chlorophyll-a algorithms for SeaWiFS, OC2, and OC4: Version 4, in: O'Reilly, J.E., and 24 co-authors: SeaWiFS Postlaunch Calibration and Validation Analyses, Part 3. *NASA Tech. Memo.* 2000-206892, Vol.11, edited by: Hooker, S. B. and Firestone, E. R., NASA Goddard Space Flight Center, Greenbelt, Maryland, 9-23.

Ridgway, K. R., J. R. Dunn, and J. L. Wilkin (2002), Ocean interpolation by four-dimensional weighted least squares: Application to the waters around Australasia, *J.*

Atmos. Oceanic Technol., *19*(9), 1357-1375.

Rouault, M., S. Illig, C. Bartholomae, C. J. C. Reason, and A. Bentamy (2007), Propagation and origin of warm anomalies in the Angola Benguela upwelling system in 2001, *Journal of Marine Systems*, *68*(3-4), 473-488.

Saha, S., et al. (2010), The NCEP climate forecast system reanalysis, *Bull. Am. Meteorol. Soc.*, *91*(8), 1015-1057.

Zabel, M. (2003), Report and Preliminary Results of METEOR Cruise M 57/2, *Walvis Bay-Walvis Bay*, *11.02-12.03.2003*, Dep. Geosci., Bremen Univ., Bremen, Germany

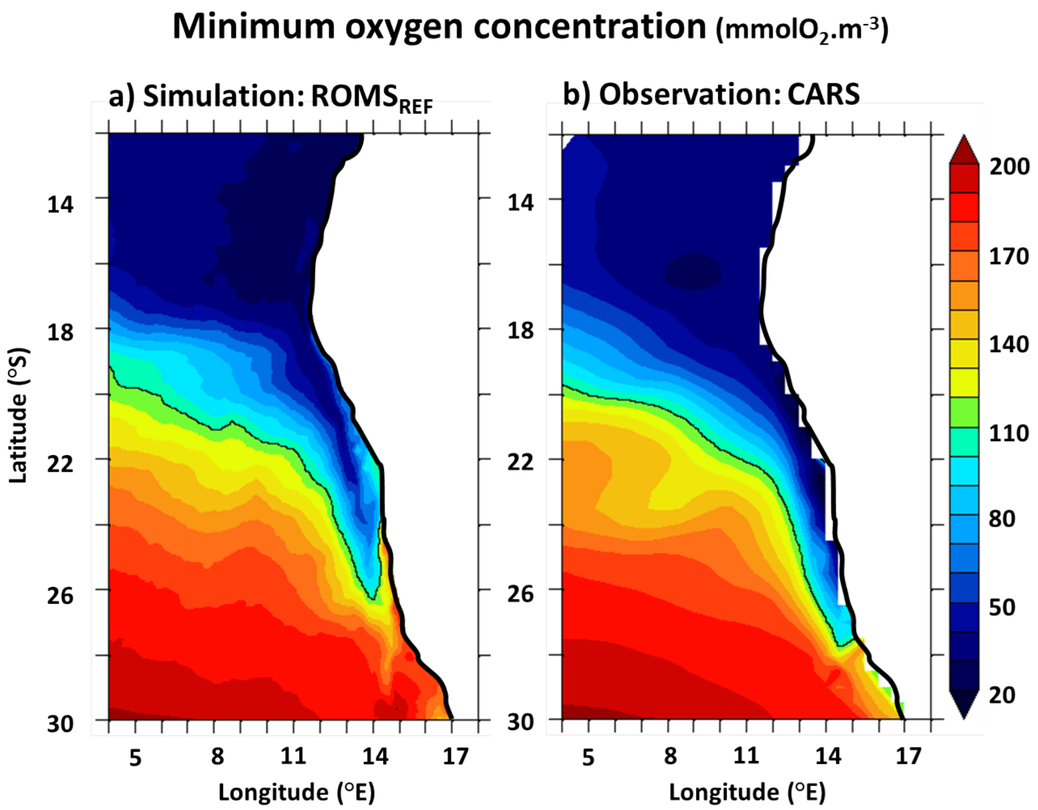

Figure S1. Maps of minimum oxygen concentration ($mmolO_2.m^{-3}$): (a) $ROMS_{REF}$ and (b) CARS climatology. Model outputs are averaged over the 2000-2008 period.

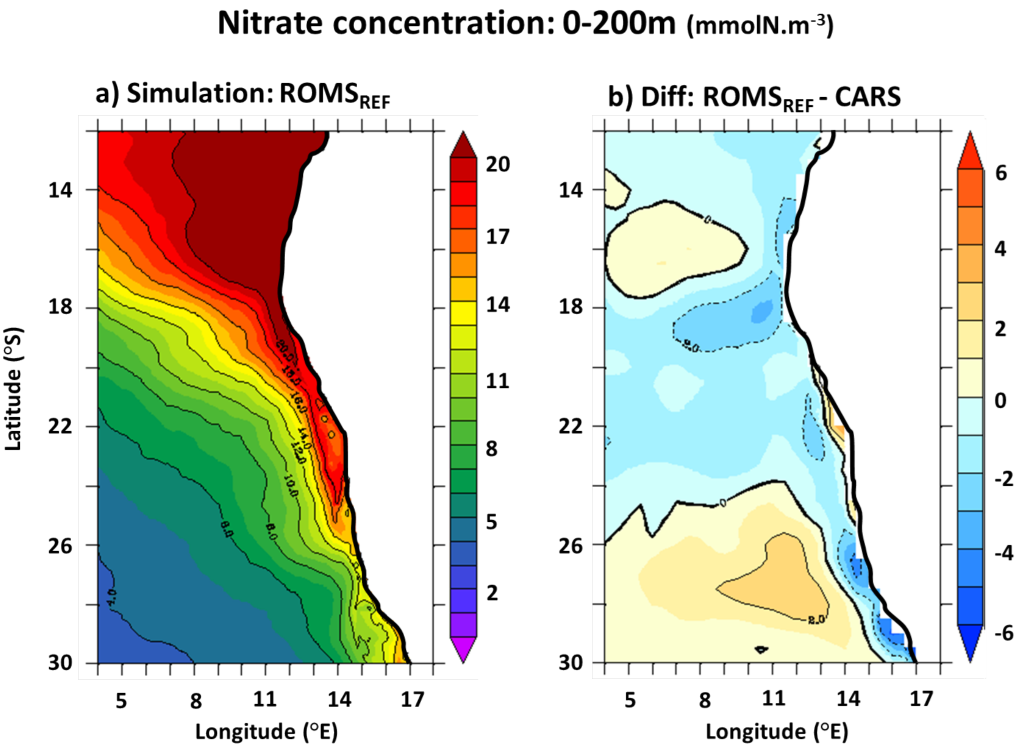

Figure S2. Maps of nitrate concentration (mmolN.m^{-3}) averaged in the first 200-meters: (a) ROMS$_{REF}$ and (b) difference between ROMS$_{REF}$ and CARS climatology. Model outputs are averaged over the 2000-2008 period.

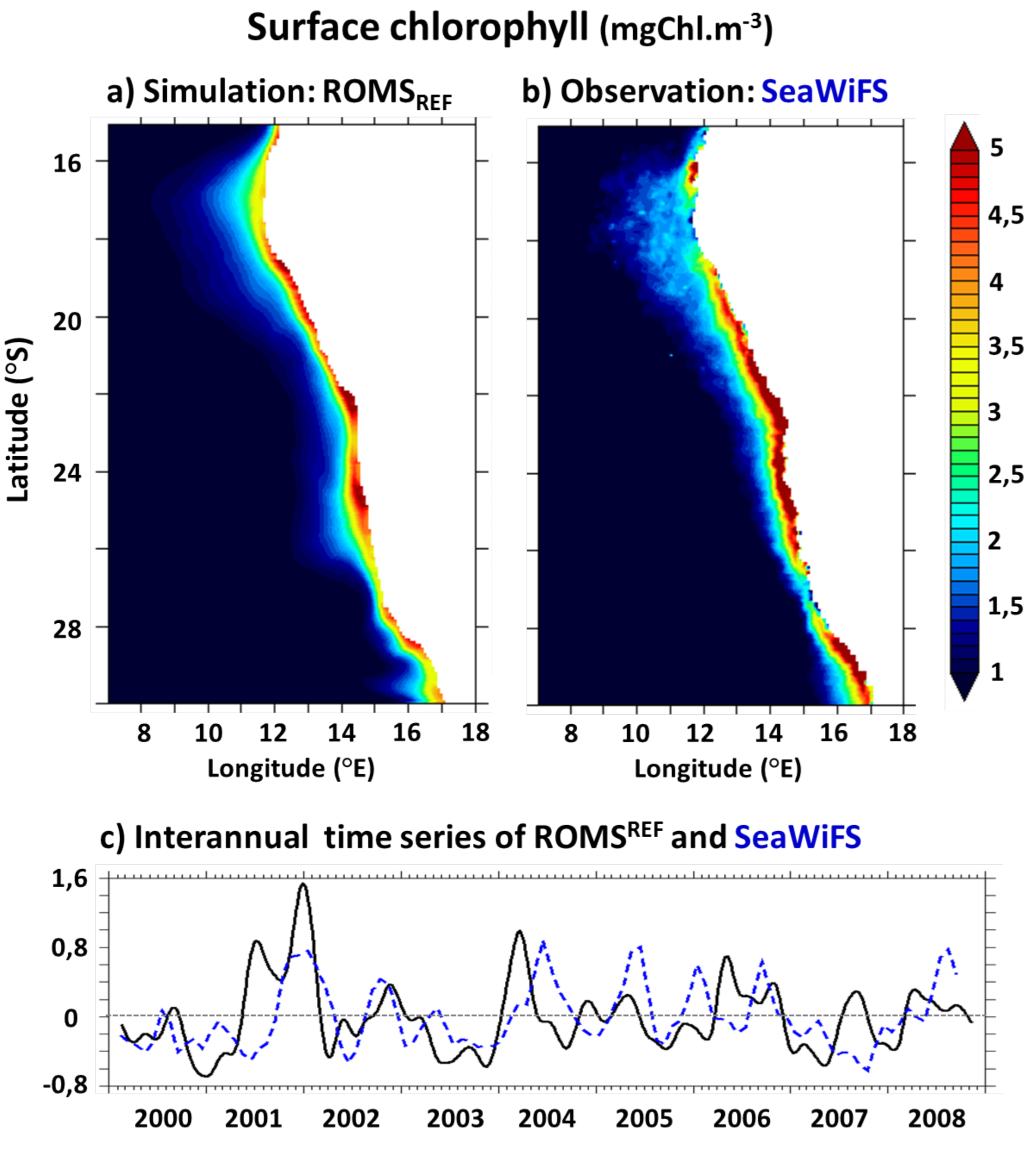

Figure S3. Surface cholorophyll-a concentration (mgChl.m^{-3}). (a-b) Maps of averaged values over the 2000-2008 period: (a) ROMS$_{REF}$ and (b) SeaWiFS satellite data. (c) Time series of interannual ROMS$_{REF}$ (black) and SeaWiFS (blue) coastal chlorophyll-a, averaged over 10°S-25°S and over 1°-width coastal band.

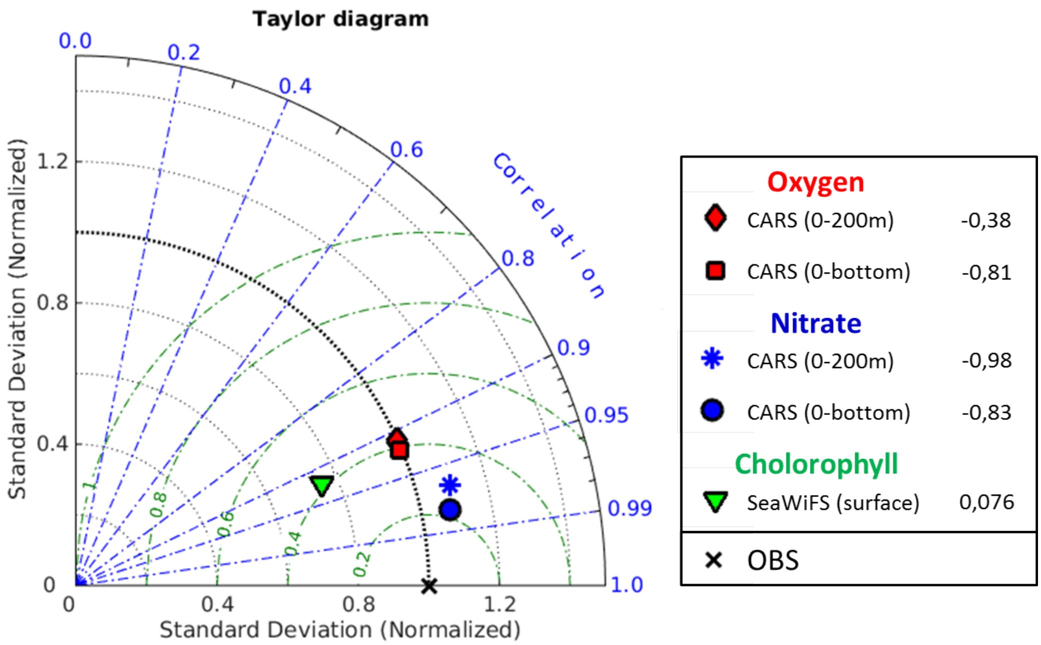

Figure S4. Taylor diagram of mean oxygen (red; $mmolO_2.m^{-3}$), nitrate (blue; $mmolN.m^{-3}$), and chlorophyll-a (green; $mgChl.m^{-3}$) concentrations: $ROMS_{REF}$ simulation skills (averaged over the 2000-2008 period) are estimated by comparison of mean maps of model outputs to corresponding maps from CARS and SeaWiFS climatologies. The radial distance from the origin is proportional to the standard deviation of a pattern (normalized by the standard deviation of the data). The green-dashed lines measure the distance from the reference point (black cross) and indicate the root mean square error. The correlation between both fields is given by the azimuthally position. Associated mean biases are given on the right of the legend. Statistics have been calculated over the whole ROMS/BioEBUS domain (7°N-30°S and 10°W-18°E) for nitrate and oxygen and over the Benguela upwelling system (19°S-28.5°S and 17°E-5°E) for chlorophyll-a.

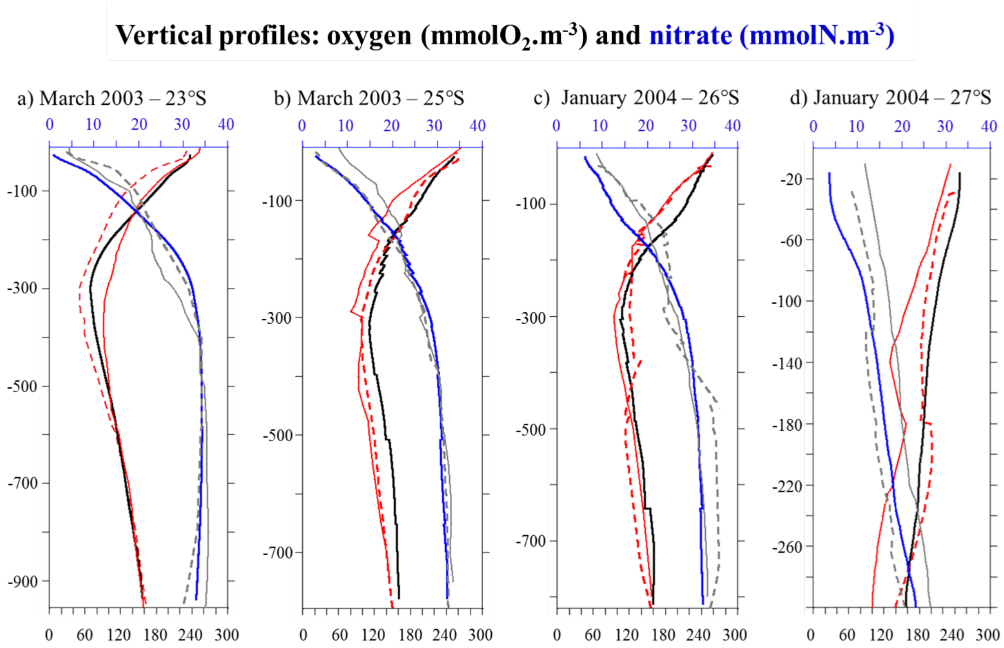

Figure S5. Vertical profiles of oxygen (black line; mmolO_2.m^{-3}) and nitrate (blue line; mmolN.m^{-3}) concentrations of $ROMS_{REF}$ simulation compared to *in situ* observations (red (oxygen) and gray (nitrate) dashed lines): the METEOR expedition 57/2 in March 2003 ((a) transects at 23°S, and (b) 25°S) and the AHAB1 expedition in January 2004 ((c) transects at 26°S) and (d) 27°S). CARS climatology data are displayed in plain red (oxygen) and gray (nitrate) lines. $ROMS_{REF}$ and CARS fields are averaged over the area and the period of the corresponding *in situ* cruise profiles.

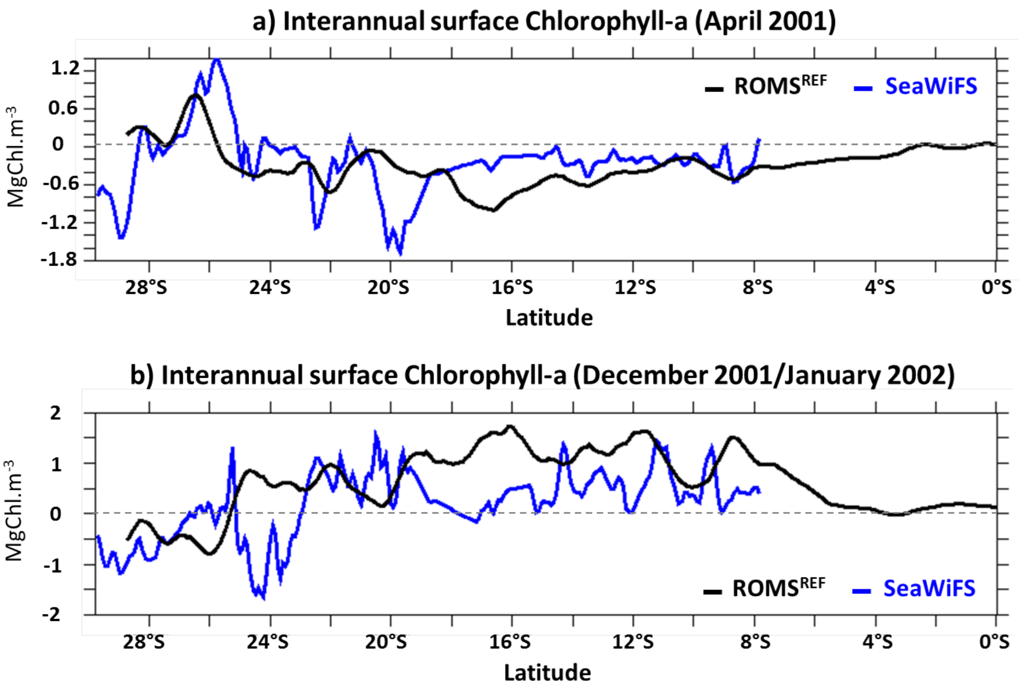

Figure S6. Latitudinal section of coastal (1°-width band) interannual surface cholorophyll-a (mgChl.m^{-3}) averaged over 1 month in (a) April 2001 and (b) 15 December 2001-15 January 2002. Black and blue lines correspond to ROMS$_{REF}$ and SeaWiFS satellite data respectively.

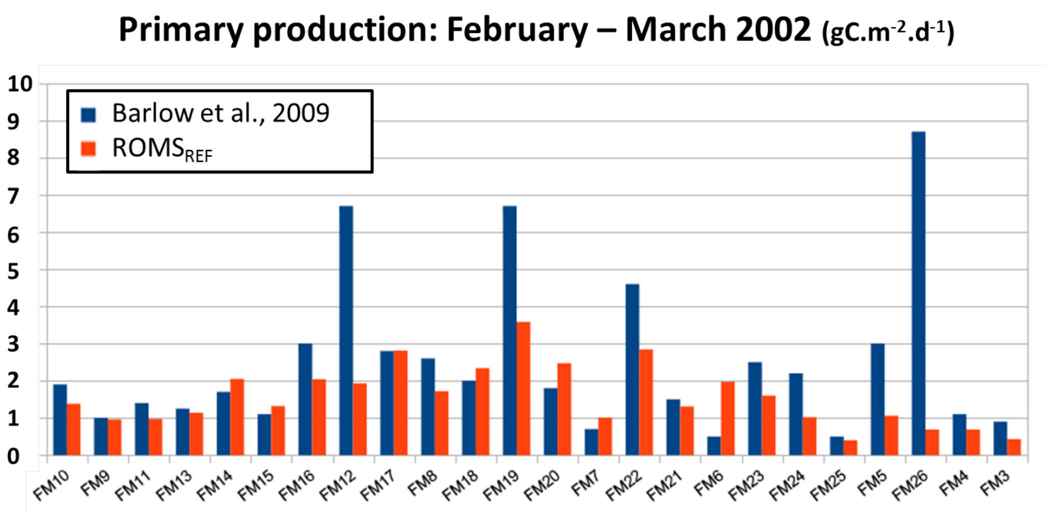

Figure S7. Primary production (gC.m^{-2}.d^{-1}) during February-March 2002 between 15°S (FM10) and 30°S (FM3) along the southwestern coast of Africa for ROMS$_{REF}$ (in red) and *in situ* data (in blue) from *Barlow et al.* [2009].